molecular pharmaceutics

Article

pubs.acs.org/molecularpharmaceutics

Generation and Screening of Monoclonal Antibodies for ImmunoPET Imaging of IGF1R in Prostate Cancer

Hao Hong,[†] Tapas R. Nayak,[†] Sixiang Shi,[‡] Stephen A. Graves,[§] Brianne C. Fliss,[∥] Todd E. Barnhart,[§] and Weibo Cai*[,†,§,⊥]

[†]Department of Radiology, [‡]Materials Science Program, [§]Department of Medical Physics, and [∥]Department of Biochemistry, University of Wisconsin—Madison, Madison, Wisconsin 53705-2275, United States

[⊥]University of Wisconsin Carbone Cancer Center, Madison, Wisconsin 53705-2275, United States

Supporting Information

ABSTRACT: Insulin-like growth factor 1 receptor (IGF1R) plays an important role in proliferation, apoptosis, angiogenesis, and tumor invasion. The expression level of IGF1R is related to resistance to several targeted therapies. The goal of this study was to develop an immunoPET tracer for imaging of IGF1R in prostate cancer. Murine antibodies against human IGF1R were generated in BALB/c mice, which were screened in IGF1R-positive MCF-7 cells using flow cytometry as well as biodistribution studies with multiple ^{64}Cu-labeled antibody clones. The antibody production method we adopted could readily produce milligram quantities of anti-IGF1R antibodies for in vivo studies. One antibody clone (1A2G11) with the highest affinity for IGF1R was selected and conjugated to NOTA for ^{64}Cu-labeling. NOTA-1A2G11 maintained IGF1R specificity/avidity based on flow cytometry. ^{64}Cu-labeling was achieved with good yield (>50%) and high specific activity (>1 Ci/μmol). Serial PET imaging revealed that uptake of ^{64}Cu-NOTA-1A2G11 was 2.8 ± 0.7, 10.2 ± 2.6, and 9.6 ± 1.7 %ID/g in IGF1R-positive DU-145 tumors at 4, 24, and 48 h postinjection, respectively (n = 3), significantly higher than that in IGF1R-negative LNCaP tumors (<3 %ID/g at each time point) except at 4 h postinjection. Histology studies showed strong correlations between IGF1R expression level in the prostate cancer tumor tissues and tumor uptake of ^{64}Cu-NOTA-1A2G11. Prominent, persistent, and IGF1R-specific uptake of ^{64}Cu-NOTA-1A2G11 in IGF1R-positive prostate tumors holds strong potential for future cancer diagnosis, prognosis, and therapy using this antibody.

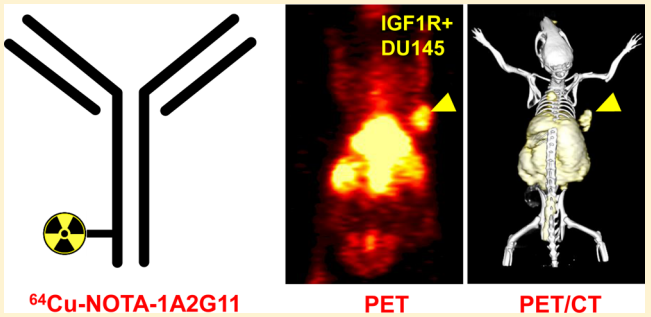

KEYWORDS: *insulin-like growth factor 1 receptor (IGF1R), positron emission tomography (PET), imaging, prostate cancer, antibody*

INTRODUCTION

Insulin-like growth factor 1 receptor (IGF1R) is a transmembrane tyrosine kinase that plays an important role in proliferation, apoptosis, angiogenesis, and tumor invasion.[1] Mounting evidence has confirmed that IGF1R is significantly upregulated in many types of cancer,[2] and the upregulation usually confers resistance to different therapeutic interventions.[3−5] These findings suggest that targeting and neutralizing IGF1R can be an effective approach for cancer therapy.[6] Different therapeutic agents such as antibodies and tyrosine kinase inhibitors have been developed for this purpose and served as effective approaches in clinical trials.[7] Inhibition of IGF1R is considered a favorable treatment for androgen-independent prostate cancer due to the fact that overexpression of IGF1R leads to activation of androgen receptors in the absence of androgens.[8]

Identification of IGF1R expression level and relevant patient stratification are the prerequisites of a successful IGF1R-targeted therapy. Clinical data also demonstrated that treatment efficacy of IGF1R antibody correlates with membrane expression of IGF1R.[9] IGF1/IGF1R signaling has been demonstrated as a determinant of prostate cancer risk.[10,11] Noninvasive imaging of IGF1R will provide invaluable information in three aspects: patient stratification where patients with high IGF1R expression can be selected for IGF1R targeted clinical trials; treatment monitoring where noninvasive imaging of IGF1R expression can indicate the therapeutic response; and facilitating the drug development process through monitoring the therapeutic efficacy of various drugs that target the IGF1R signaling pathway. At the same time, the expression level of IGF1R in tumor is comparatively low (10^4 to 3×10^4 receptors per cell[12]), and physiological IGF1R expression exists in a number of tissues, such as colon, lung, pancreas, salivary gland, and stomach, although the expression level in those tissues is significantly lower than in

Received: May 16, 2014
Revised: July 31, 2014
Accepted: August 26, 2014
Published: August 26, 2014

tumor.[13] The combination of low tumor expression and ubiquitous expression in normal tissues posed a challenge to acquiring accurate IGF1R profiles. This dilemma was partially resolved with the utilization of radionuclide-based imaging techniques, including single-photon emission computed tomography (SPECT) and positron emission tomography (PET), because these modalities can achieve superior sensitivity (down to picomolar level) and are highly quantitative.[14] SPECT imaging studies of IGF1R in prostate cancer were conducted using an affibody molecule;[13,15] however, there is no PET imaging of IGF1R reported to date for prostate cancer.

Monoclonal antibodies (mAbs) have long been considered promising candidates for targeted therapy and diagnostics due to their highly specific targeting ability: they offer unmatched utility by virtue of their ability to recognize essentially any target of interest.[16] The goal of this study was to develop a mAb (named 1A2G11) for IGF1R and investigate the in vitro and in vivo characteristics of ^{64}Cu-labeled 1A2G11 for PET imaging of IGF1R in different prostate cancer models. We hypothesized that the uptake of ^{64}Cu-labeled 1A2G11 in these prostate tumors are dependent on their IGF1R expression level.

EXPERIMENTAL SECTION

Production of Monoclonal Antibodies Against Human IGF1R. The production of IGF1R mAbs was carried out by Neoclone Biotechnologies International, LLC (Madison, WI). Briefly, the production procedure involved four major steps: (1) screening of peptidic immunogens for IGF1R, (2) immunization in BALB/c female mice with IGF1R immunogens, (3) identification of IGF1R-positive cell candidates through serial screening of different monoclonal colonies from hybridomas, and (4) bulk production of the most promising candidate. Approximately 10 peptidic immuogens were screened using bioinformatical calculation based on the structure of human IGF1R.[17] BALB/c female mice were inoculated with recombinant mouse protein with sequences of IGF1R immunogens. Enzyme-linked immunosorbent assay (ELISA) was initially prepared with immobilized IGF1R. Ten to 20 clones of IGF1R-positive cells with the highest read-outs in ELISA were used to carry out flow cytometry assay. Then, three clones with the highest cellular affinity for IGF1R were radiolabeled with ^{64}Cu and applied for in vivo biodistribution assay. The antibody clone with the highest uptake in IGF1R-positive tumors (1A2G11) was produced in a milligram scale.

Flow Cytometry. The binding affinity of different antibody clones for IGF1R was evaluated with fluorescence-activated cell sorting (FACS) analysis in MCF-7 human breast cancer cells (IGF1R-positive[18,19]). Cells were harvested and suspended in cold phosphate buffered saline (PBS) with 2% bovine serum albumin at a concentration of 5×10^6 cells/mL. The cells were incubated with supernatants from different cell clones (total protein concentration: 50 μg/mL based on Bradford protein assay, which contains ~0.5 μg/mL of antibodies) for 30 min at room temperature and washed three times with cold PBS at the end of the incubation period. They were then incubated with FITC-labeled rabbit antimouse IgG (1 μg/mL) for 30 min at room temperature. Subsequently, the cells were washed and analyzed using a BD FACSCalibur 4-color analysis cytometer, which is equipped with 488 and 633 nm lasers (Becton-Dickinson, San Jose, CA). Mean fluorescence intensities of different antibody clones in the cells were computed using FlowJo analysis software (Tree Star, Inc., Ashland, OR).

Tumor-Bearing Mouse Model. All animal studies were conducted under a protocol (M02239) approved by University of Wisconsin Institutional Animal Care and Use Committee. Tumors were established by subcutaneous injection of 5×10^6 DU-145 (IGF1R-positive[13]) or LNCaP cells (IGF1R-negative[20]) suspended in 100 μL of 1:1 mixture of PBS and Matrigel (BD Biosciences, Franklin lakes, NJ) into the right front flank of male nude mice purchased from Harlan (Indianapolis, IN). The tumor sizes were monitored every other day, and the mice were subjected to in vivo experiments when the diameter of tumors reached 6−8 mm (typically 4−6 weeks after inoculation).

PET Imaging and Biodistribution Studies. PET scans were performed using an Inveon microPET/microCT rodent model scanner (Siemens Medical Solutions USA, Inc.). Each tumor-bearing mouse was injected with 5−10 MBq of the PET tracer via its tail vein and subjected to 5−15 min of static PET scans at various time points postinjection (p.i.). The images were reconstructed using a maximum a posteriori (MAP) algorithm, with no attenuation or scatter correction. For each microPET scan, three-dimensional (3D) regions-of-interest (ROIs) were superimposed on the tumor and major organs in the decay-corrected whole-body images by using a vendor software (Inveon Research Workshop [IRW]). Assuming a tissue density of 1 g/mL, the radioactivity in each ROI volume was converted to MBq/g using a conversion factor, and then divided by the total administered radioactivity to obtain a percentage of injected dose per gram of tissue (%ID/g) for each ROI.

To anatomically localize the radioactivity signal observed in PET, several test subjects also underwent microCT scans. Immediately after PET scanning, a sample set of mice were transported to the microCT gantry, positioned, and scanned at a voxel resolution of 210 μm (scanning time: 7 min). CT images were reconstructed using the vendor software (Inveon Acquisition Workshop; Siemens) using fiducial markers for coregistration. The microCT and microPET data sets were loaded into IRW where the corresponding fiducial markers were coregistered to achieve ROI location alignment.

Biodistribution studies were carried out to confirm that the quantitative tracer uptake values based on PET imaging truly represented the radioactivity distribution in tumor-bearing mice. After the last PET scans at 48 h p.i., the mice were euthanized, and their blood, DU-145/LNCaP tumors, and major organs/tissues were collected and wet-weighed. The radioactivity in each collected sample was measured using a WIZARD^2 automatic gamma-counter (PerkinElmer) and recorded as %ID/g (mean ± SD). The DU-145/LNCaP tumors, liver, and spleen (i.e., tissues with significant uptake of ^{64}Cu-labeled antibodies) were also frozen for histological analysis.

Histology. Frozen tissue slices of 5 μm thickness were fixed with cold acetone for 10 min and air-dried at room temperature for 30 min. After rinsing with PBS and blocking with 10% donkey serum for 30 min at room temperature, the slices were incubated with antibody 1A2G11 (5 μg/mL) for 1 h at 4 °C and visualized using FITC-labeled rabbit antimouse secondary antibody. The tissue slices were also stained for endothelial marker CD31. After washing with PBS, the tissue slices were incubated with rat antimouse CD31 antibody (2 μg/mL) for 1 h, followed by Cy3-labeled donkey antirat IgG for 30 min. All images were taken with a Nikon Eclipse Ti microscope.

dx.doi.org/10.1021/mp5003637 | Mol. Pharmaceutics 2014, 11, 3624−3630

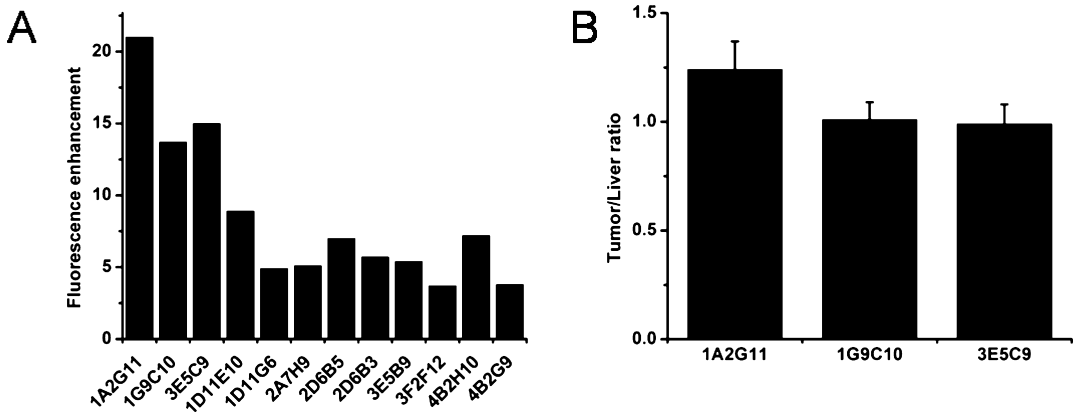

Figure 1. (A) Fluorescence enhancement of IGF1R-positive MCF-7 cells measured by FACS analysis after treatment with supernatants of different monoclonal colonies. (B) Tumor-to-liver ratios of ^{64}Cu-labeled 1A2G11, 1G9C10, and 3E5C9 in DU-145 tumor bearing mice (n = 2).

Statistical Analysis. Data were presented in the format of mean ± SD. Means were compared using Student's t test. P values <0.05 were considered statistically significant.

RESULTS

Screening/Production of 1A2G11. Multiple rounds of screening were carried out on different monoclonal colonies to select antibodies with the highest affinity for IGF1R on MCF-7 (Figure S1, Supporting Information). Candidate ranking was based on cellular fluorescence intensity levels from FACS measurement in descending order; the final candidates were 1A2G11, 1G9C10, and 3E5C9 (Figure 1A). The immunoglobin G (IgG) contents from these three clones were purified and enriched to a final concentration of 0.1−0.5 mg/mL for NOTA conjugation and ^{64}Cu-labeling. ^{64}Cu-labeled 1A2G11, 1G9C10, and 3E5C9 were injected into DU-145 tumor bearing mice (n = 2) to evaluate their distribution pattern and tumor-targeting efficacy in vivo by gamma-counting measurement (Figure S2, Supporting Information). A comparison of tumor-to-liver uptake ratio for the three candidates (Figure 1B) indicated that 1A2G11 possesses the highest tumor-targeting capability; therefore, it was selected for the subsequent studies. Further enrichment and purification steps were undertaken to acquire 1A2G11 antibody at the final concentration of 1 mg/mL.

In Vitro Investigation of NOTA-1A2G11. Cell binding assays confirmed that 50% inhibitory concentration (IC_{50}) of 1A2G11 for MCF-7 cells (which expressed high level of IGF1R) was around 5 nM, confirming its high affinity for IGF1R (Figure S4, Supporting Information). Data from FACS analysis in MCF-7 suggested no observable difference in cellular binding affinity between 1A2G11 and NOTA-1A2G11 at the concentration of 5 μg/mL. The binding to MCF-7 was antigen specific, as neither 1A2G11 nor NOTA-1A2G11 bound to IGF1R-negative LNCaP cells, even at a much higher concentration of 20 μg/mL (Figure 2). In aggregation, FACS analysis data indicated that NOTA conjugation did not alter the antigen binding affinity or specificity of 1A2G11.

Radiolabeling and Small Animal PET Imaging. The ^{64}Cu-labeling procedure, including final purification using PD-10 columns, was completed within 100 ± 10 min (n = 7). The estimated ^{64}Cu-NOTA-1A2G11 specific activity was ~0.75 GBq/mg protein (assuming full protein recovery after size-exclusion chromatography), a result based on the calculation of 25 μg of NOTA-1A2G11 per 37 MBq of ^{64}Cu and an decay-corrected radiochemical yield of 51 ± 15%.

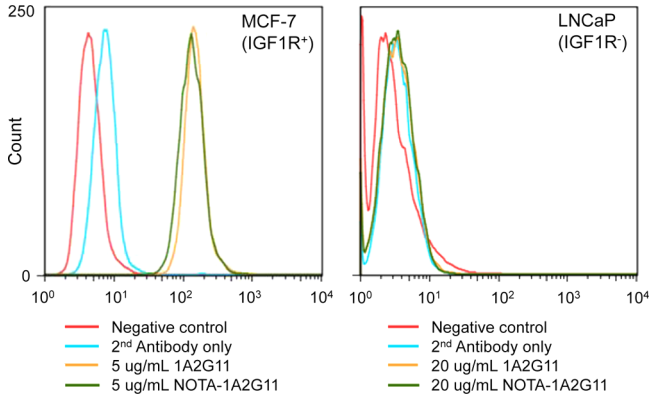

Figure 2. Flow cytometry analysis of 1A2G11 and NOTA-1A2G11 in MCF-7 (IGF1R-positive) and LNCaP (IGF1R-negative) cells at different concentrations.

Drawing on our prior experiences in PET imaging with ^{64}Cu-labeled antibodies,[21,22] sample time points of 4, 24, and 48 h p.i. were chosen for serial PET scans after intravenous tracer injection. Reconstructed coronal slices that contained the DU-145 or LNCaP tumors are shown in Figure 3A; a representative PET/CT fused image of a DU-145 tumor-bearing mouse at 24 h p.i. of ^{64}Cu-NOTA-1A2G11 is shown in Figure 3B. Quantitative data obtained from ROI analysis at the 3 time points are graphed in Figure 3C. Blood pool activity was prominent at early time points and gradually declined thereafter (10.3 ± 1.9, 7.4 ± 0.9, and 4.1 ± 0.6 %ID/g at 4, 24, and 48 h p.i., respectively, n = 3). The liver uptake of ^{64}Cu-NOTA-1A2G11 in DU-145 tumor-bearing mice displayed the same trend (20.2 ± 2.1, 15.2 ± 0.8, and 12.8 ± 0.6 %ID/g at 4, 24, and 48 h p.i., respectively, n = 3). Most significantly, the uptake of ^{64}Cu-NOTA-1A2G11 in DU-145 tumor was clearly visible as early as 4 h p.i. and the level plateaued at around 24 h p.i. (2.8 ± 0.7, 10.2 ± 2.6, and 9.6 ± 1.7 %ID/g at 4, 24, and 48 h p.i., respectively; n = 3; Figure 3A,C).

To further investigate IGF1R specificity of ^{64}Cu-NOTA-1A2G11, the LNCaP tumor, which does not express detectable level of IGF1R, was selected as a control model. The uptake of ^{64}Cu-NOTA-1A2G11 in LNCaP was very low (1.7 ± 0.8, 2.8 ± 0.7, and 2.2 ± 0.6 %ID/g at 4, 24, and 48 h p.i., respectively; n = 3; Figure 3A). The liver uptake (18.2 ± 1.8, 16.7 ± 1.4, and 10.2 ± 0.9 %ID/g at 4, 24, and 48 h p.i., respectively) and the blood radioactivity (10.6 ± 1.3, 6.8 ± 1.5, and 3.5 ± 0.7 %ID/g

dx.doi.org/10.1021/mp5003637 | Mol. Pharmaceutics 2014, 11, 3624−3630

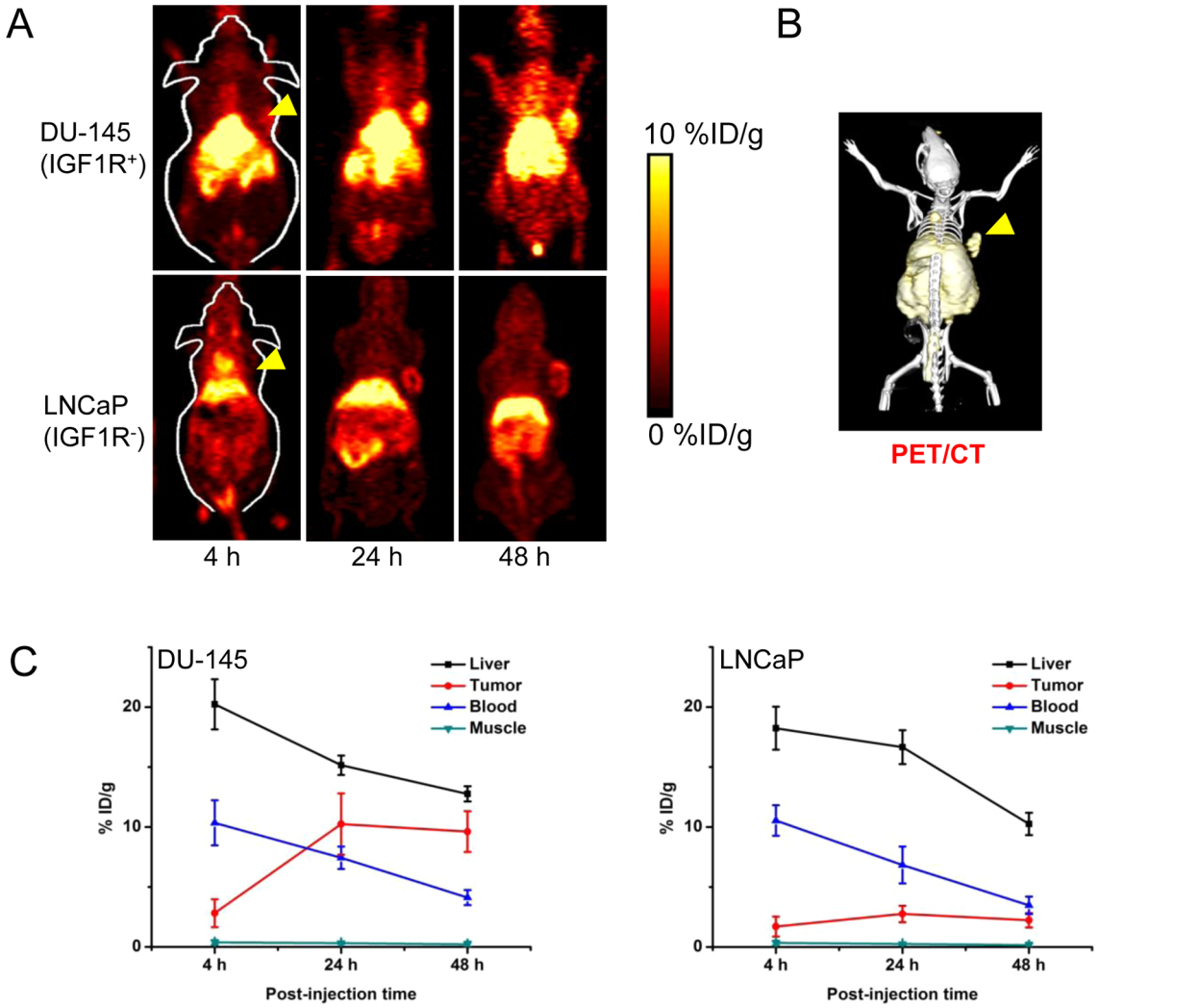

Figure 3. Serial PET imaging and ROI quantifications of IGF1R in DU-145 and LNCaP tumor-bearing mice. (A) Serial coronal PET images of DU-145 and LNCaP tumor-bearing mice at 4, 24, and 48 h postinjection of ^{64}Cu-NOTA-1A2G11. (B) Representative PET/CT image of ^{64}Cu-NOTA-1A2G11 in DU-145 tumor-bearing mice at 24 h p.i. (C) Time−activity curves of the tumor, liver, blood, and muscle upon intravenous injection of ^{64}Cu-NOTA-1A2G11 into DU-145 or LNCaP tumor-bearing mice (n = 3).

at 4, 24, and 48 h p.i., respectively; n = 4; Figure 3A) were similar to those in DU-145 tumor model.

An additional group of two mice were each injected with DU-145 cells on the right flank and LNCaP cells on the left flank and subjected to serial ^{64}Cu-NOTA-1A2G11 PET scans. While significant uptake of ^{64}Cu-NOTA-1A2G11 in the DU-145 tumors could be observed at 24 h p.i., tracer uptake in the LNCaP tumors was at a significantly lower level (Figure S3, Supporting Information). Noninvasive detection of IGF1R-positive tumors but not IGF1R-negative tumors in the same mice further validated that ^{64}Cu-NOTA-1A2G11 can specifically target IGF1R in vivo.

Biodistribution Studies. All mice were euthanized after the terminal PET scans at 48 h p.i. for biodistribution and histology studies to validate the in vivo PET data. Tumors, blood, liver, and spleen of the test subjects also had significant radioactivity accumulation at 48 h p.i., an expected condition since a radiolabeled antibody typically has long circulation half-life and hepatic clearance (Figure 4). Appreciable tracer uptake (~5%ID/g) in the kidney was also detected, an observation likely attributed to a small fraction of ^{64}Cu detaching from NOTA-1A2G11 and possible tracer degradation over time

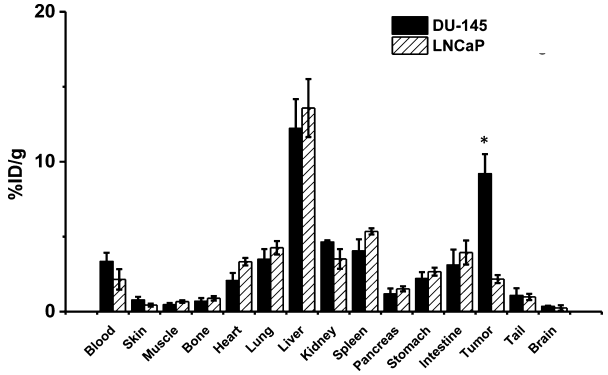

Figure 4. Biodistribution of ^{64}Cu-NOTA-1A2G11 in DU-145 or LNCaP tumor-bearing mice at 48 h postinjection (n = 3). *P < 0.05.

(lower molecular weight species can undergo renal clearance). DU-145/LNCaP tumor-bearing mice showed similar ^{64}Cu-NOTA-1A2G11 biodistribution profile in all the major organs/tissues except the tumor. Uptake of ^{64}Cu-NOTA-1A2G11 in the DU-145 tumor was significantly higher than in the LNCaP

dx.doi.org/10.1021/mp5003637 | Mol. Pharmaceutics 2014, 11, 3624−3630

control model. Comparisons of ^{64}Cu-NOTA-1A2G11 uptake levels in all major organs to that of the DU-145 tumor have also suggested that excellent tumor contrast can be achieved in muscle tissue with a tumor/muscle ratio of 20.3 ± 2.1 at 48 h p.i. (n = 3).

Histology. Immunofluorescence IGF1R/CD31 staining revealed that IGF1R expression was prominent on the DU-145 tumor cells, but weak on the LNCaP cells (Figure 5).

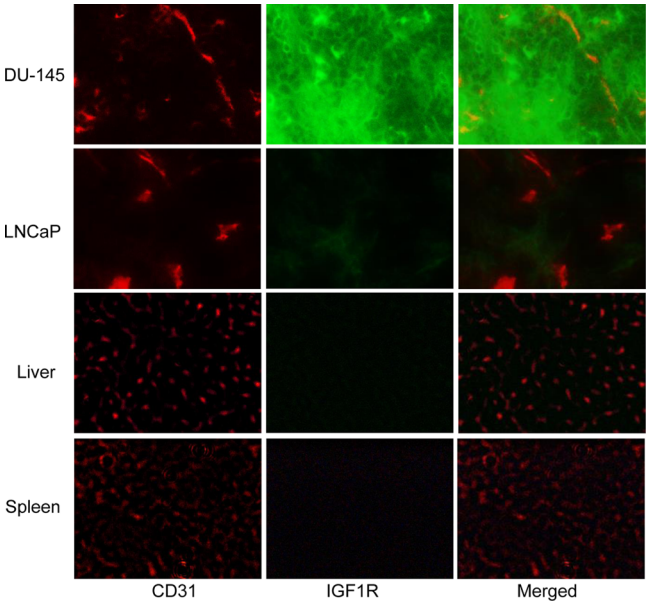

Figure 5. Immunofluorescence IGF1R/CD31 double-staining of the DU-145 or LNCaP tumor, liver, and spleen tissue sections. 1A2G11 and FITC-labeled goat antimouse IgG were used for IGF1R staining (green). Subsequently, the tissue slices were stained with rat antimouse CD31 antibody and Cy3-labeled donkey antirat IgG (red). All images were acquired under the same conditions and displayed on the same scale. Magnification: 200×.

IGF1R staining of mouse liver/spleen/muscle all produced very low signal because these tissues do not express IGF1R at a high level, and the binding affinity of 1A2G11 to murine IGF1R is low. Therefore, uptake of ^{64}Cu-NOTA-1A2G11 in mouse liver/spleen was largely unrelated to IGF1R binding and more likely related to nonspecific capture by the reticuloendothelial system and hepatic clearance of the tracer.

DISCUSSION

IGF1R is overexpressed in most cancer types. Mounting literature data have suggested a key role for IGF1R in the development and metastasis of cancer.[23] Currently, several small-molecule inhibitors and antibodies directed against the IGF-1R are being developed and tested in phase I and II clinical trials. Preliminary results of these studies have demonstrated the safety and tolerability of targeting IGF1R.[24] Objective responses have been reported in patients treated with these new agents, but the relationship between treatment efficacy and IGF1R expression is still poorly understood. In order to identify patients who may benefit from IGF-1R target therapy, reliable biomarkers must be developed to predict patient responses. One basis for patient selection is receptor expression. Histology evaluation of tumor samples would be the most accurate approach to stratify patients for this purpose; however, this method cannot be used to measure the expression in different tumor lesions or at different regions within a tumor. This level of discernment would require multiple invasive sampling procedures. Furthermore, the expression of IGF1R may change with time as the result of tumor growth, therapy, or other circumstances. Radionuclide imaging offers an alternative that allows repeated noninvasive evaluation of IGF1R both for patient stratification and for monitoring expression-level changes in response to therapy. The present study developed a noninvasive imaging method that can be applicable for monitoring of the membranous IGF-1R expression in prostate cancer.

Multiple groups have performed imaging of IGF1R in cancer using agents ranging from peptides to antibodies,[13,19,25−28] among which radiolabeled antibodies demonstrated highest tumor-to-background ratios. Novel PET tracers for various purposes such as detection of receptor abundance[29] or tumor environment,[30] monitoring of therapy response,[31,32] or locating apoptosis sites,[33] are actively pursued by various research groups. Over the past decade, a myriad of preclinical and clinical data has suggested that immunoPET holds great potential for managing cancer in patients.[16] The advantages of antibody-based tracers are high antigen specificity, high binding affinity, and absolute tumor uptake; these are characteristics that make them suitable for internal radiotherapy applications and/or targeted delivery of anticancer drugs. Major limitations of antibody-based imaging are slow tumor accumulation and high background signal in the reticuloendothelial system; these drawbacks may be circumvented by employing peptide, small molecule, or antibody fragment-based tracers. Although antibodies with high affinity for IGF1R have already been developed (e.g., R1507,[26] IMC-A12,[34] etc.), PET imaging with ^{64}Cu-NOTA-1A2G11 can monitor therapeutic responses of these antibodies in patients without the possible interference of "blocking" effects caused by excessive antibody in the bloodstream.

In this study, we have successfully developed and characterized ^{64}Cu-labeled IGF1R antibody (^{64}Cu-NOTA-1A2G11) for PET imaging of tumor IGF1R expression in vivo. The main advantages of ^{64}Cu-NOTA-1A2G11 are its specific accumulation in the tumor and its comparatively rapid clearance from the circulation. In vitro experiments were performed to compare the IGF1R binding characteristics of 1A2G11 and NOTA-1A2G11. Overall, NOTA conjugation did not compromise the IGF1R binding affinity of 1A2G11. Our data showed that ^{64}Cu-NOTA-1A2G11 specifically bound to IGF1R-positive DU-145 tumors but not to IGF1R-negative LNCaP tumors, and the tumor uptake of ^{64}Cu-NOTA-1A2G11 was closely associated with IGF1R expression level in the tumor. Even on the same test subject, ^{64}Cu-NOTA-1A2G11 can delineate and differentiate tumors with different IGF1R expression (Figure S3, Supporting Information). Such IGF1R specificity in vivo makes ^{64}Cu-NOTA-1A2G11 a PET tracer with broad potential applications in many clinical situations. One limitation of ^{64}Cu-NOTA-1A2G11 lies in its moderate uptake in IGF1R-positive tumors when compared with commercially available IGF1R antibodies (e.g., R1507,[26] typically have an uptake of more than 20 %ID/g in IGF1R-positive tumors), which is partially due to its short circulation half-life. Engineering of 1A2G11 (e.g., affinity maturation, multimerization, site mutation, etc.[35]) or further screening from the antibody library will bring hope to overcome this limitation in the future. To gain further insight on the long-term behavior of 1A2G11 in vivo, other long-lived isotopes (e.g., ^{89}Zr, which

has a decay half-life of 3.3 days[36]) can be explored in future studies.

Since PET scanners detect the distribution of ^{64}Cu rather than the antibody itself, a key requirement for accurate PET imaging with ^{64}Cu-labeled antibodies is that the tracer should be sufficiently stable during the imaging period. NOTA is generally recognized as one of the best chelators for ^{64}Cu-labeling. A recent study that compared the effect of several bifunctional chelators on the biodistribution of a ^{64}Cu-labeled antibody[37] has concluded that the thermodynamic stability of ^{64}Cu-chelator complexes did not significantly influence tumor uptake of the tracer, but did dramatically affect the normal tissue distribution.

Our studies have demonstrated the feasibility of ^{64}Cu-NOTA-1A2G11 PET for in vivo imaging of IGF1R expression. However, these experiments were performed under optimal conditions because 1A2G11 does not cross react with the murine IGF1R. In patients, radiolabeled 1A2G11 will also recognize IGF1R that is widely expressed in normal tissues, including muscle, cartilage, and bone.[38−40] This may skew test results by enhancing IGF1R uptake in expressing normal tissues.[15] Future studies to optimize imaging of IGF1R expression with 1A2G11 will be required in patients.

CONCLUSIONS

Herein we report the development, characterization, and in vivo investigation of ^{64}Cu-labeled IGF1R mAb (1A2G11) in mouse models of prostate tumors with different expression levels of IGF1R. ^{64}Cu-labeled 1A2G11 exhibited rapid, prominent, and target-specific uptake in IGF1R-positive tumors while demonstrating minimal interaction with IGF1R-negative tumors. PET imaging can evaluate the pharmacokinetics, tumor targeting efficacy, and dose optimization of 1A2G11, preparing it for future IGF1R-targeted cancer therapeutics in the clinic.

ASSOCIATED CONTENT

Supporting Information

Detailed methods and results for antibody screening, biodistribution, PET imaging, and cell binding assay. This material is available free of charge via the Internet at http://pubs.acs.org.

AUTHOR INFORMATION

Corresponding Author

*(W.C.) Departments of Radiology and Medical Physics, University of Wisconsin—Madison, Room 7137, 1111 Highland Avenue, Madison, Wisconsin 53705-2275, United States. E-mail: wcai@uwhealth.org. Phone: 608-262-1749. Fax: 608-265-0614.

Notes

The authors declare no competing financial interest.

ACKNOWLEDGMENTS

This work is supported, in part, by the University of Wisconsin—Madison, the National Institutes of Health (NIBIB/NCI 1R01CA169365 and P30CA014520), the Department of Defense (W81XWH-11-1-0644), and the American Cancer Society (125246-RSG-13-099-01-CCE).

REFERENCES

(1) Pollak, M. N.; Schernhammer, E. S.; Hankinson, S. E. Insulin-like growth factors and neoplasia. *Nat. Rev. Cancer* **2004**, *4*, 505−18.

(2) Zhang, Y.; Cai, W. Molecular imaging of insulin-like growth factor 1 receptor in cancer. *Am. J. Nucl. Med. Mol. Imaging* **2012**, *2*, 248−259.

(3) Nahta, R.; Yuan, L. X.; Zhang, B.; Kobayashi, R.; Esteva, F. J. Insulin-like growth factor-I receptor/human epidermal growth factor receptor 2 heterodimerization contributes to trastuzumab resistance of breast cancer cells. *Cancer Res.* **2005**, *65*, 11118−28.

(4) Wu, J. D.; Haugk, K.; Coleman, I.; Woodke, L.; Vessella, R.; Nelson, P.; Montgomery, R. B.; Ludwig, D. L.; Plymate, S. R. Combined in vivo effect of A12, a type 1 insulin-like growth factor receptor antibody, and docetaxel against prostate cancer tumors. *Clin. Cancer Res.* **2006**, *12*, 6153−60.

(5) Thomas, F.; Holly, J. M.; Persad, R.; Bahl, A.; Perks, C. M. Fibronectin confers survival against chemotherapeutic agents but not against radiotherapy in DU145 prostate cancer cells: involvement of the insulin like growth factor-1 receptor. *Prostate* **2010**, *70*, 856−65.

(6) Bruchim, I.; Attias, Z.; Werner, H. Targeting the IGF1 axis in cancer proliferation. *Expert Opin. Ther. Targets* **2009**, *13*, 1179−92.

(7) Weroha, S. J.; Haluska, P. IGF-1 receptor inhibitors in clinical trials–early lessons. *J. Mammary Gland Biol. Neoplasia* **2008**, *13*, 471−83.

(8) Antonarakis, E. S.; Carducci, M. A.; Eisenberger, M. A. Novel targeted therapeutics for metastatic castration-resistant prostate cancer. *Cancer Lett.* **2010**, *291*, 1−13.

(9) Haluska, P.; Shaw, H. M.; Batzel, G. N.; Yin, D.; Molina, J. R.; Molife, L. R.; Yap, T. A.; Roberts, M. L.; Sharma, A.; Gualberto, A.; Adjei, A. A.; de Bono, J. S. Phase I dose escalation study of the anti insulin-like growth factor-I receptor monoclonal antibody CP-751,871 in patients with refractory solid tumors. *Clin. Cancer Res.* **2007**, *13*, 5834−40.

(10) Hellawell, G. O.; Turner, G. D.; Davies, D. R.; Poulsom, R.; Brewster, S. F.; Macaulay, V. M. Expression of the type 1 insulin-like growth factor receptor is up-regulated in primary prostate cancer and commonly persists in metastatic disease. *Cancer Res.* **2002**, *62*, 2942−50.

(11) Ryan, C. J.; Haqq, C. M.; Simko, J.; Nonaka, D. F.; Chan, J. M.; Weinberg, V.; Small, E. J.; Goldfine, I. D. Expression of insulin-like growth factor-1 receptor in local and metastatic prostate cancer. *Urol. Oncol.* **2007**, *25*, 134−40.

(12) Zha, J.; O'Brien, C.; Savage, H.; Huw, L. Y.; Zhong, F.; Berry, L.; Lewis Phillips, G. D.; Luis, E.; Cavet, G.; Hu, X.; Amler, L. C.; Lackner, M. R. Molecular predictors of response to a humanized anti-insulin-like growth factor-I receptor monoclonal antibody in breast and colorectal cancer. *Mol. Cancer Ther.* **2009**, *8*, 2110−21.

(13) Tolmachev, V.; Malmberg, J.; Hofstrom, C.; Abrahmsen, L.; Bergman, T.; Sjoberg, A.; Sandstrom, M.; Graslund, T.; Orlova, A. Imaging of insulinlike growth factor type 1 receptor in prostate cancer xenografts using the affibody molecule ^{111}In-DOTA-ZIGF1R:4551. *J. Nucl. Med.* **2012**, *53*, 90−7.

(14) James, M. L.; Gambhir, S. S. A molecular imaging primer: modalities, imaging agents, and applications. *Physiol. Rev.* **2012**, *92*, 897−965.

(15) Orlova, A.; Hofstrom, C.; Strand, J.; Varasteh, Z.; Sandstrom, M.; Andersson, K.; Tolmachev, V.; Graslund, T. $[^{99m}Tc(CO)_3]^+$-(HE)3-ZIGF1R:4551, a new Affibody conjugate for visualization of insulin-like growth factor-1 receptor expression in malignant tumours. *Eur. J. Nucl. Med. Mol. Imaging* **2013**, *40*, 439−49.

(16) Wu, A. M. Antibodies and antimatter: the resurgence of immuno-PET. *J. Nucl. Med.* **2009**, *50*, 2−5.

(17) Ullrich, A.; Gray, A.; Tam, A. W.; Yang-Feng, T.; Tsubokawa, M.; Collins, C.; Henzel, W.; Le Bon, T.; Kathuria, S.; Chen, E.; et al. Insulin-like growth factor I receptor primary structure: comparison with insulin receptor suggests structural determinants that define functional specificity. *EMBO J.* **1986**, *5*, 2503−12.

(18) Zhang, H.; Zeng, X.; Li, Q.; Gaillard-Kelly, M.; Wagner, C. R.; Yee, D. Fluorescent tumour imaging of type I IGF receptor in vivo: comparison of antibody-conjugated quantum dots and small-molecule fluorophore. *Br. J. Cancer* **2009**, *101*, 71−9.

(19) Heskamp, S.; van Laarhoven, H. W.; Molkenboer-Kuenen, J. D.; Bouwman, W. H.; van der Graaf, W. T.; Oyen, W. J.; Boerman, O. C. Optimization of IGF-1R SPECT/CT imaging using ^{111}In-labeled F(ab′)$_2$ and Fab fragments of the monoclonal antibody R1507. *Mol. Pharmaceutics* **2012**, *9*, 2314−21.
(20) Nickerson, T.; Chang, F.; Lorimer, D.; Smeekens, S. P.; Sawyers, C. L.; Pollak, M. In vivo progression of LAPC-9 and LNCaP prostate cancer models to androgen independence is associated with increased expression of insulin-like growth factor I (IGF-I) and IGF-I receptor (IGF-IR). *Cancer Res.* **2001**, *61*, 6276−80.
(21) Hong, H.; Yang, Y.; Zhang, Y.; Engle, J. W.; Barnhart, T. E.; Nickles, R. J.; Leigh, B. R.; Cai, W. Positron emission tomography imaging of CD105 expression during tumor angiogenesis. *Eur. J. Nucl. Med. Mol. Imaging* **2011**, *38*, 1335−43.
(22) Hong, H.; Zhang, Y.; Nayak, T. R.; Engle, J. W.; Wong, H. C.; Liu, B.; Barnhart, T. E.; Cai, W. Immuno-PET of tissue factor in pancreatic cancer. *J. Nucl. Med.* **2012**, *53*, 1748−54.
(23) Hartog, H.; Wesseling, J.; Boezen, H. M.; van der Graaf, W. T. The insulin-like growth factor 1 receptor in cancer: old focus, new future. *Eur. J. Cancer* **2007**, *43*, 1895−904.
(24) Gualberto, A.; Pollak, M. Emerging role of insulin-like growth factor receptor inhibitors in oncology: early clinical trial results and future directions. *Oncogene* **2009**, *28*, 3009−21.
(25) Fleuren, E. D.; Versleijen-Jonkers, Y. M.; Heskamp, S.; Roeffen, M. H.; Bouwman, W. H.; Molkenboer-Kuenen, J. D.; van Laarhoven, H. W.; Oyen, W. J.; Boerman, O. C.; van der Graaf, W. T. The strength of small: improved targeting of insulin-like growth factor-1 receptor (IGF-1R) with F(ab′)$_2$-R1507 fragments in Ewing sarcomas. *Eur. J. Cancer* **2013**, *49*, 2851−8.
(26) Fleuren, E. D.; Versleijen-Jonkers, Y. M.; van de Luijtgaarden, A. C.; Molkenboer-Kuenen, J. D.; Heskamp, S.; Roeffen, M. H.; van Laarhoven, H. W.; Houghton, P. J.; Oyen, W. J.; Boerman, O. C.; van der Graaf, W. T. Predicting IGF-1R therapy response in bone sarcomas: immuno-SPECT imaging with radiolabeled R1507. *Clin. Cancer Res.* **2011**, *17*, 7693−703.
(27) Heskamp, S.; van Laarhoven, H. W.; Molkenboer-Kuenen, J. D.; Franssen, G. M.; Versleijen-Jonkers, Y. M.; Oyen, W. J.; van der Graaf, W. T.; Boerman, O. C. ImmunoSPECT and immunoPET of IGF-1R expression with the radiolabeled antibody R1507 in a triple-negative breast cancer model. *J. Nucl. Med.* **2010**, *51*, 1565−72.
(28) Majo, V. J.; Arango, V.; Simpson, N. R.; Prabhakaran, J.; Kassir, S. A.; Underwood, M. D.; Bakalian, M.; Canoll, P.; John Mann, J.; Dileep Kumar, J. S. Synthesis and in vitro evaluation of [^{18}F]BMS-754807: a potential PET ligand for IGF-1R. *Bioorg. Med. Chem. Lett.* **2013**, *23*, 4191−4.
(29) Zhang, X. X.; Sun, Z.; Guo, J.; Wang, Z.; Wu, C.; Niu, G.; Ma, Y.; Kiesewetter, D. O.; Chen, X. Comparison of ^{18}F-labeled CXCR4 antagonist peptides for PET imaging of CXCR4 expression. *Mol. Imaging Biol.* **2013**, *15*, 758−67.
(30) Lopci, E.; Grassi, I.; Chiti, A.; Nanni, C.; Cicoria, G.; Toschi, L.; Fonti, C.; Lodi, F.; Mattioli, S.; Fanti, S. PET radiopharmaceuticals for imaging of tumor hypoxia: a review of the evidence. *Am. J. Nucl. Med. Mol. Imaging* **2014**, *4*, 365−84.
(31) Guo, J.; Guo, N.; Lang, L.; Kiesewetter, D. O.; Xie, Q.; Li, Q.; Eden, H. S.; Niu, G.; Chen, X. ^{18}F-alfatide II and ^{18}F-FDG dual-tracer dynamic PET for parametric, early prediction of tumor response to therapy. *J. Nucl. Med.* **2014**, *55*, 154−60.
(32) Li, Z.; Herrmann, K.; Pirsig, S.; Philipp-Abbrederis, K.; Henninger, M.; Aichler, M.; Feuchtinger, A.; Walch, A.; Beer, A. J.; Ringshausen, I.; Pomykala, K. L.; Scheidhauer, K.; Schwaiger, M.; Keller, U.; Buck, A. K. Molecular imaging for early prediction of response to Sorafenib treatment in sarcoma. *Am. J. Nucl. Med. Mol. Imaging* **2013**, *4*, 70−9.
(33) Wang, F.; Wang, Z.; Hida, N.; Kiesewetter, D. O.; Ma, Y.; Yang, K.; Rong, P.; Liang, J.; Tian, J.; Niu, G.; Chen, X. A cyclic HSV1-TK reporter for real-time PET imaging of apoptosis. *Proc. Natl. Acad. Sci. U.S.A.* **2014**, *111*, 5165−70.
(34) Ma, C. X.; Suman, V. J.; Goetz, M.; Haluska, P.; Moynihan, T.; Nanda, R.; Olopade, O.; Pluard, T.; Guo, Z.; Chen, H. X.; Erlichman, C.; Ellis, M. J.; Fleming, G. F. A phase I trial of the IGF-1R antibody Cixutumumab in combination with temsirolimus in patients with metastatic breast cancer. *Breast Cancer Res. Treat.* **2013**, *139*, 145−53.
(35) Maynard, J.; Georgiou, G. Antibody engineering. *Annu. Rev. Biomed. Eng.* **2000**, *2*, 339−76.
(36) Hong, H.; Severin, G. W.; Yang, Y.; Engle, J. W.; Zhang, Y.; Barnhart, T. E.; Liu, G.; Leigh, B. R.; Nickles, R. J.; Cai, W. Positron emission tomography imaging of CD105 expression with ^{89}Zr-Df-TRC105. *Eur. J. Nucl. Med. Mol. Imaging* **2012**, *39*, 138−48.
(37) Dearling, J. L.; Voss, S. D.; Dunning, P.; Snay, E.; Fahey, F.; Smith, S. V.; Huston, J. S.; Meares, C. F.; Treves, S. T.; Packard, A. B. Imaging cancer using PET: the effect of the bifunctional chelator on the biodistribution of a ^{64}Cu-labeled antibody. *Nucl. Med. Biol.* **2011**, *38*, 29−38.
(38) Philippou, A.; Halapas, A.; Maridaki, M.; Koutsilieris, M. Type I insulin-like growth factor receptor signaling in skeletal muscle regeneration and hypertrophy. *J. Musculoskeletal Neuronal Interact.* **2007**, *7*, 208−18.
(39) Karna, E.; Miltyk, W.; Surazynski, A.; Palka, J. A. Protective effect of hyaluronic acid on interleukin-1-induced deregulation of beta1-integrin and insulin-like growth factor-I receptor signaling and collagen biosynthesis in cultured human chondrocytes. *Mol. Cell. Biochem.* **2008**, *308*, 57−64.
(40) Massicotte, F.; Aubry, I.; Martel-Pelletier, J.; Pelletier, J. P.; Fernandes, J.; Lajeunesse, D. Abnormal insulin-like growth factor 1 signaling in human osteoarthritic subchondral bone osteoblasts. *Arthritis Res. Ther.* **2006**, *8*, R177.